Journal of Materials Chemistry A

RSC Publishing

PAPER

View Article Online
View Journal | View Issue

Cite this: J. Mater. Chem. A, 2013, 1, 8790

Structure evolution and SERS activation of cuprous oxide microcrystals *via* chemical etching†

Chao Qiu, Ying Bao, Nathan L. Netzer and Chaoyang Jiang*

The morphology, composition, and structure of semiconductor nanomaterials play important roles in tuning their unique physical and chemical properties for a variety of applications. We report a facile chemical method to etch cuprous oxide microcrystals which resulted in excellent performance in surface-enhanced Raman scattering (SERS). Microscopic and spectroscopic tools were utilized to investigate the cuprous oxide structures with the chemical etching, as well as the assessment of the SERS sensitivity. The increasing SERS sensitivity can be attributed to the generation of Raman hot spots related to the etching-induced rough surface, sharp tips and edges, as well as the strong chemical interactions between the probe molecules and the SERS substrates. Our work introduced a simple method to modify the semiconductor nanomaterials and induce SERS activity, thus expanding the application area of cuprous oxide microcrystals.

Received 7th April 2013
Accepted 20th May 2013

DOI: 10.1039/c3ta11395g

www.rsc.org/MaterialsA

Introduction

Semiconductor materials have demonstrated an increasing interest in both fundamental studies and practical applications; especially those related to tunable band gaps and optical properties when their dimensions are on the scale of nanometers. As a typical semiconductor with a bulk band gap of 2.2 eV, cuprous oxide (Cu_2O) is a multi-functional material that can be utilized in broad applications such as low-cost photovoltaics,[1–3] photocatalysis,[4,5] and gas sensors.[6,7] The properties of Cu_2O are largely dependent on their nano- or microstructures. Cu_2O with well controlled morphologies have been synthesized, ranging from cubic,[8,9] octahedral,[9,10] truncated octahedral[11] to truncated rhombic dodecahedral,[11] nanowires,[12] and porous nanostructures.[13,14] Such various morphologies result in interesting catalytic, electrical, photocatalytic, optical, and molecular adsorption properties. For example, Wang and Zhang studied structure-dependent optical responses by tailoring the radii of Cu_2O nanoshells.[15] Dai and co-workers reported a photodegradation of dye molecules using Cu_2O microcrystals with well-formed facets.[16] Furthermore, post-synthetic chemical modifications are considered important alternatives to tune the micro- and nanostructures.[17,18] Cu_2O nanocubes were oxidized to urchin-like particles and an excellent electrochemical performance was revealed, which is critical for lithium battery application.[19] The Cu_2O nanocubes can also be used as nanotemplates to prepare other nanomaterials for improving the lithium storage capability.[20] Overall, post-synthesis modification provides a new means to tune structures of semiconductor nanomaterials, which offers additional opportunities for multi-step structural optimizations and performance improvements.[21–25]

Surface-enhanced Raman scattering (SERS) has attracted increasing attention due to its broad applications ranging from ultrasensitive chemical identification,[26,27] biological sensing,[28–31] environmental analysis[32] to space exploration and homeland security.[33] The current on-going SERS study includes substrate design,[34–36] experimental fabrication,[37–39] and theoretical modelling.[40–42] Among various SERS substrates, noble metal based nanostructures[43–45] have received much attention since their surface plasmon resonance can largely enhance the local electromagnetic field and SERS signals. Recently, SERS-active substrates composed of transition metals[46] and semiconducting materials[47,48] have been explored. The SPRs of semiconductors and quantum dots have been discovered in the near infrared range.[49,50] A systematic study of the semiconductor SERS substrates will not only facilitate an insightful understanding of SERS, but also extend the selection of SERS substrates, broaden the range of SERS applications, and create new applications for semiconductor nanomaterials.

The SERS capability of cuprous oxide was first investigated by Dolata and co-workers.[51] The SERS activity of nanoscale cuprous oxide was recently reported and its enhancement mechanism was tentatively elucidated.[26,52,53] For instance, plasma-etched Cu_2O porous nanowires,[52] Cu_2O nanospheres,[26] and Cu_2O related nanodendrites[53] were reported for the enhanced SERS abilities. Besides that, SERS-active substrates also include Cu_2O nano-structural materials, and Cu related materials, such as

Department of Chemistry, University of South Dakota, Vermillion, South Dakota 57069, USA. E-mail: Chaoyang.Jiang@usd.edu; Fax: +1 605 677 6397; Tel: +1 605 677 6250

† Electronic supplementary information (ESI) available: Additional TEM micrographs, preparation of LB films, and long-term SERS stability tests. See DOI: 10.1039/c3ta11395g

Ag–CuO thin films[54] and Cu nanoparticle colloidals.[55] In our previous study, we reported that Cu_2O porous nanostructures exhibited excellent SERS sensitivity, which can be attributed to both electromagnetic (EM) field enhancement and photo-induced charge transfer (CT) enhancement.[56] On the other hand, a variety of studies on Cu_2O submicro- or microparticles have been conducted, ranging from their various tunable structures to their structure-dependent properties. Cu_2O microstructures have the potential to be utilized as SERS substrates. As far as we know, so far there has been no report on the SERS activity obtained directly from Cu_2O microcrystals.

In this article, we introduce a facile chemical approach to create Raman hot spots on Cu_2O microcrystals, which can consequently generate impressive SERS activities. The Cu_2O microcrystals were chemically etched using an ammonia solution. During the etching process, the morphologies of those Cu_2O microcrystals were altered; their optical properties were widely tuned; and the SERS capabilities were largely improved. SERS signals were obtained from chemically modified Cu_2O microcrystals, and the enhancements were largely related to the reaction time and pH values of the etchants. Our results provide a new opportunity to use SERS to explore the molecule–semiconductor interaction, a fundamental but essential question for designing novel devices.

Methods

Synthesis of Cu_2O microcrystals

The Cu_2O microcrystals were synthesized according to a previously reported method.[57] Typically, 0.825 g of copper chloride dihydrate (Acros 99%) was first dissolved in 50 mL of deionized water under constant stirring. 10 mL of NaOH (6.0 mol L^{-1}) aqueous solution was added dropwise to the copper chloride solution. The resulting mixture was continuously stirred for five minutes at a constant temperature of 70 °C. Then, 0.200 g of D-glucose powder was added to the mixture, and the reaction mixture was kept at 70 °C and stirred for 15 minutes. During this process, the precipitate gradually changed its color from blue to brick red. The reaction mixture was then naturally cooled down to room temperature and the precipitates were centrifuged and washed several times using deionized water and methanol. The resulting microcrystals were finally dispersed in methanol for further experiments.

Thin film fabrication and etching

Two types of thin films of cuprous oxide microcrystals were prepared in our experiments. The Langmuir–Blodgett (LB) technique was employed to fabricate uniform Cu_2O microcrystal thin films. More information about LB film preparation can be found in the ESI.† A drop casting method was used to prepare Cu_2O thin films with low-density microcrystals. For the chemical etching process, those thin films were dipped into ammonia solutions with different pH values for desired times. In most cases, the microcrystal thin films were treated with ammonia solution (pH = 11.7), unless otherwise specified (ranging from 11.2 to 11.9). After etching, the thin films were thoroughly washed using deionized water and methanol, and were dried under nitrogen stream. For enhanced Raman measurements, 10 μL (0.8 mmol L^{-1}) of 4-aminothiophenol (4-ATP) solution was well spread on the prepared Cu_2O microcrystal thin films and dried naturally.

Characterizations

The structural evolution of microcrystals in the thin films was studied using scanning electron microscopy (SEM) and transmission electron microscopy (TEM). SEM images, obtained from a Zeiss Supra40VP variable-pressure field-emission SEM, were employed to investigate the morphologies of Cu_2O microcrystals. Furthermore, microstructures were examined using TEM on a FEI Tecnai electron microscope with an acceleration voltage of 120 kV. We also utilized an X-ray photoelectron spectrometer (XPS) to study the variation of the chemical composition during the etching process. The XPS (ESCA SSX-100) was equipped with a monochromated Al K_α X-ray source, a hemispherical sector analyzer (HSA) and a resistive anode detector. The base pressure of the XPS system was 5.0×10^{-10} Torr. During the data collection, the pressure was *ca.* 5×10^{-9} Torr. The X-ray spot size was 1×1 mm^2, which corresponded to an X-ray power of 200 W. Absorbance spectra of Cu_2O microcrystals and their thin films were measured using a Cary 50 UV-Vis spectrophotometer.

SERS spectra and confocal Raman mapping were collected on an Aramis confocal Raman microscope (Horiba Jobin Yvon, Edison, NJ) equipped with a diode-pump solid state (DSPP) laser (532 nm). The laser with an intensity of 0.40 mW was focused using a 50× objective (NA 0.75) onto the samples on the glass slides, which were mounted onto a $200 \times 200 \times 200$ μm piezo scanner. The Raman signals were collected with the same objective lens at a 180° back-scattering configuration and passed through an edge filter into a monochromator and an electric-cooled charge-coupled device (CCD) camera. For single crystal Raman spectrum, the acquisition time was five seconds. To obtain a Raman map, a selected area of the sample was raster scanned under the laser beam and an array of the Raman spectra was recorded with an acquisition time of one second for each position. The spectra were then mathematically processed, and the intensity distribution for the Raman peaks of interest can be revealed.

Results and discussion

Chemical etching with ammonium solutions can be clearly revealed by the change of colors for Cu_2O microcrystals. Fig. 1a shows the digital photographs of a Cu_2O microcrystal thin film before and after the ammonia solution treatment. The color change of the thin film was noticeable, which indicates the occurrence of chemical etching and the possibility of producing new morphologies and chemical compositions (Fig. 1a right).

To further investigate the optical properties of Cu_2O microcrystals in the etching process, *in situ* UV-Vis spectra were recorded as shown in Fig. 1b. The spectra were collected with a

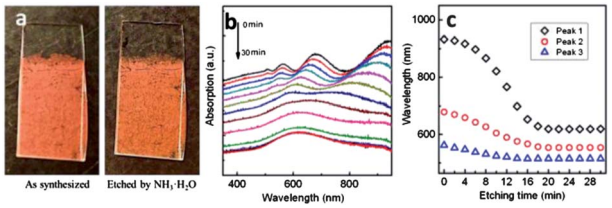

Fig. 1 (a) Photographic images of as-synthesized Cu_2O, and that reacted with ammonia solution; (b) *in situ* UV-Vis spectra of the Cu_2O microcrystal thin film reacted with $NH_3 \cdot H_2O$ solution. Each spectrum was recorded after every two minutes; (c) change of the positions of the Cu_2O microcrystal thin film extinction peaks during the reaction.

time interval of two minutes. The Cu_2O microcrystals exhibit four scattering peaks at 508, 564, 677, and 935 nm. Those scattering peaks originate from the phase-retardation effect as was discussed in the literature.[58,59] During the chemical etching, those scattering peaks showed a trend of significant blue shift, and eventually exhibited a broad peak at about 625 nm. The absorption spectra might be partially affected by dissolved copper ions in ammonia solution, since the color of the reactant solution changed to light blue after 30 min reaction. The broad peak can be due to the scattering of numerous irregular Cu_2O microcrystals. Moreover, the absorption intensities gradually decreased with the progress of the etching reaction. That is reasonable because some of the Cu_2O microcrystals were etched off from the thin film and, as a result, the amount of Cu_2O was reduced.

Fig. 1c shows the positions of the main scattering peaks for the Cu_2O microcrystals during the etching reaction. It is clear that the peak positions blue shifted during the etching reaction. The reaction was eventually finished after 20 min etching. Similarly, a study on the absorption intensity also gives a conclusion that there was no obvious decrease in the UV-Vis extinction spectra for Cu_2O microcrystal thin films after 20 min reaction. For a structural and optical study of the etched Cu_2O microcrystals, the reaction time was kept under 30 minutes since the etching processes are most likely completed in such a time period.

The morphology changes of Cu_2O microcrystals during the chemical etching were investigated using scanning electron microscopy. As shown in Fig. 2a, the as-synthesized Cu_2O microcrystals display uniform octahedral crystal shapes with tiny truncated corners. Those crystals with an edge length of about 1 μm were packed on the glass substrates. The SEM images showed crystal facets with a smooth surface. Those microcrystals exhibit uniform size, and are well spread without any agglomeration during the thin film preparation. When reacted with $NH_3 \cdot H_2O$ solution, those microcrystals gradually altered their morphologies upon the on-going etching process. Several etch pits around 50 nm can be observed on the (111) facets of the Cu_2O microcrystals reacted for five minutes (Fig. 2b). The dimension, depth, and density of etch pits increased with a longer etch period, and the roughness of facets also increased as shown in Fig. 2c and d. After 20 min reaction, some (111) facets were even completely etched off and microcrystal octahedron structures were partially broken, which left irregular hollow structures, a rough surface, and few sharp edges (Fig. 2e). Most crystal structures eventually broke into parts with 30 min etching (Fig. 2f), resulting in irregular thin shells and broken pieces with sharp edges.

The morphology and crystal structure of Cu_2O microcrystals were also investigated using TEM, from which the changes in shape and crystallinity during the etching process are clearly observed (Fig. 3). While the as-synthesized Cu_2O microcrystals have smooth edges in the TEM image (Fig. 3a), the edges of the etched microcrystals (10 min) are rougher (Fig. 3b). Such non-smooth edges can be observed more obviously in Fig. 3c where an individual microcrystal is imaged. The High Resolution TEM (HRTEM) of the edge portion clearly reveals a crystal lattice fringe of 0.25 nm, which is corresponding to the *d*-spacing of (111) planes of $Cu(OH)_2$ crystals or $(1\bar{1}1)$ planes of CuO crystals. After a 20 min reaction, sharp tips and irregular features were observed on the microcrystal surface as shown in Fig. S1,† which indicated the continuous etching reaction.

The chemical etching process not only altered the shape of the Cu_2O microcrystals, but also changed the chemical components and produced new copper species. A reaction mechanism has been proposed by Huang *et al.* where the surface of the etched Cu_2O microcrystal is converted to a mixture of Cu_2O, CuO and $Cu(OH)_2$ according to known reactions.[60] The chemical composition variations of Cu_2O microcrystals were further studied *via* an X-ray photoelectron spectroscopy technique. XPS is considered to be a powerful

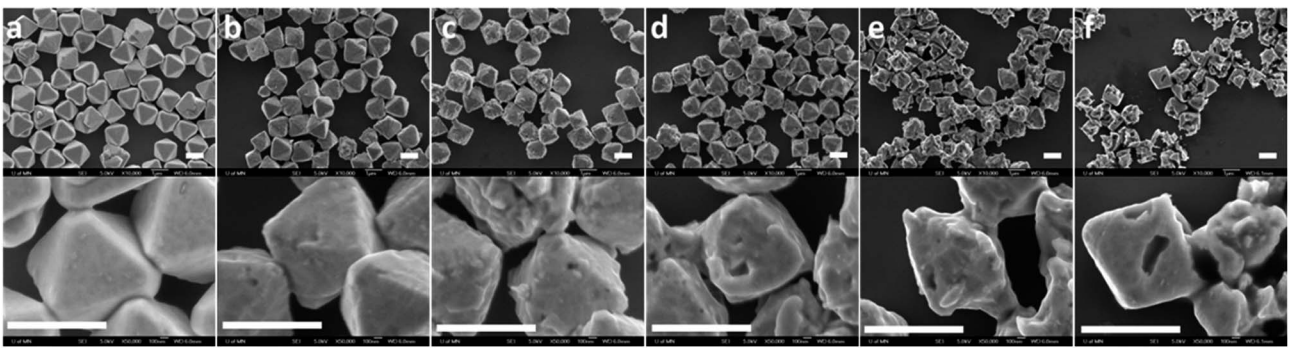

Fig. 2 SEM images of Cu_2O microcrystal thin films reacted with ammonia solution (pH = 11.7) under different reaction conditions. (a)–(f) represent the reaction time differences: 0, 5, 10, 15, 20, 30 min, respectively. The detailed morphology is shown in the higher resolution SEM images in the bottom row. All scale bars are 1 μm.

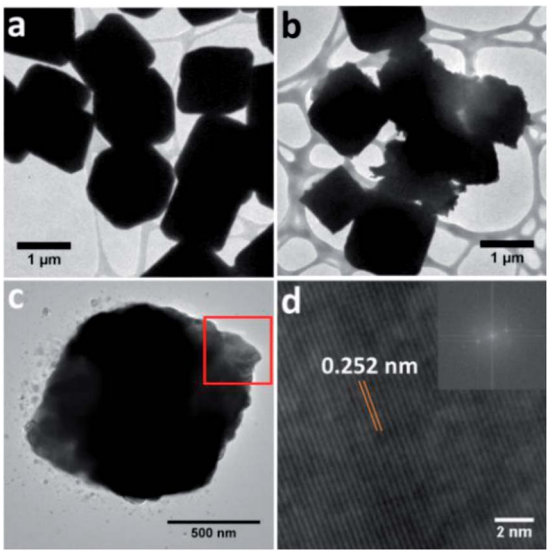

Fig. 3 TEM micrographs of as-synthesized Cu_2O microcrystals (a), and Cu_2O crystals etched 10 min by ammonia solution (pH = 11.7). (c) Magnified TEM image of a Cu_2O microcrystal etched 10 min by ammonia solution (pH = 11.7). (d) HRTEM image corresponding to the marked area in (c) and its fast Fourier transform pattern (inset).

technique to study the transition metal compounds. As shown in Fig. 4a, a strong Cu $2p_{3/2}$ peak at 932.2 eV is observed in the XPS spectrum of as-synthesized Cu_2O microcrystals. This peak can be attributed to Cu(I) which represents the formation of Cu_2O.[61,62] A few shake-up satellite peaks were also observed in the spectra, which are related to the diagnostic features of an open $3d^9$ shell. Those satellite peaks are corresponding to Cu(II) states at high binding energies of 934.6, 941.4, and 943.8 eV, respectively.[62] The appearance of shake-up satellite peaks of as-synthesized Cu_2O microcrystals might result from the amorphous Cu(II) due to surface oxidation. This phenomenon has also been reported in the literature.[63]

The chemically etched Cu_2O microcrystals exhibited different XPS spectral patterns as compared to the as-synthesized ones. The positions of copper peaks remain unchanged with the ongoing etching process (Fig. 4a). However, the relative intensities of various copper peaks showed significant changes (Fig. 4b). For the 10 min etching, the positions of copper peaks remained the same while the relative intensity of the peak at 932.2 eV decreased dramatically. Such a decrease in the peak intensity was further observed in the samples after 20 min etching. This is quite reasonable considering the solubility of Cu_2O microcrystals in ammonia solution during the etching process. With the progress of the etching reaction, Cu(I) ions on the microcrystal facets were further dissolved, and Cu(II) ions were formed. After 20 min etching, the amount of Cu(II) ions on the surface of microcrystals eventually exceeded the amount of Cu(I). Knowing the changes in chemical composition can be very helpful in controlling the structure and morphology of the resulting particles, which can play important roles in determining their optical characteristics and applications such as SERS.

SERS spectra and maps of Cu_2O microcrystals with different etching times were measured to study the impact of chemical etching on their SERS activities. As we know, quantitative studies of the enhancement factor (EF) of designed SERS substrates, as well as their uniformity and reproducibility, have become tremendously critical in developing new materials for ultra-sensitive SERS detection. In our case, we employed 4-ATP as probe molecules to assess the SERS activities of the as-synthesized Cu_2O microcrystals (1.0 mol L^{-1} 4-ATP) and etched Cu_2O microcrystals (4×10^{-5} mol L^{-1} 4-ATP). Three photographs shown in Fig. 5 were taken after the deposition of probe molecules on the microcrystal substrates. In the sample of as-synthesized Cu_2O microcrystals, a grey area was observed around the scattered microcrystals which can be due to the high concentration of the 4-ATP solution. In the corresponding Raman map (Fig. 5d), a weak Raman intensity domain can be observed and the domain shape is very similar to that in the photograph, confirming the existence of the 4-ATP molecules. Furthermore, the presence of Cu_2O microcrystals did not promote strong Raman signals. Even with a high 4-ATP concentration, only infinitesimal Raman signals can be recognized from those as-synthesized Cu_2O microcrystals. This result is consistent with our previous report on the size dependent SERS activities of cuprous oxide materials.[56]

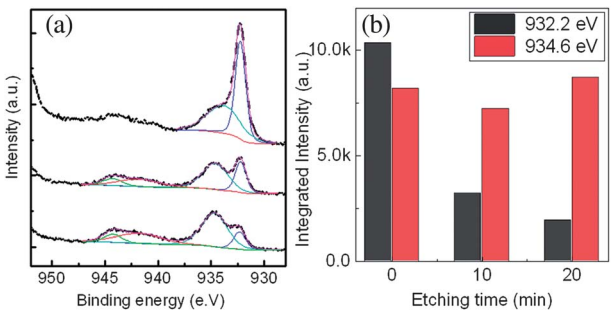

Fig. 4 (a) XPS spectra of Cu_2O microcrystals reacted with $NH_3 \cdot H_2O$ (pH = 11.7) for different times, from top to bottom: 0, 10, and 20 min. (b) Comparison on integrated areas of Cu^+ and Cu^{2+} peaks.

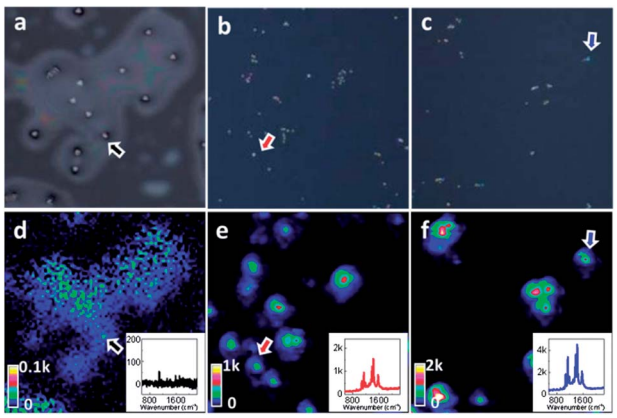

Fig. 5 Bright field optical photographs (a–c) of as-synthesized Cu_2O microcrystals, etched by $NH_3 \cdot H_2O$ solution (pH = 11.9) for 5 and 10 min, respectively. Sizes of the area shown in the photographs: 40 × 40 μm. Raman maps (d–f) represent the corresponding area in optical images. Inset: the SERS spectra acquired from the positions that were pointed out by the colored arrows, respectively.

On the other hand, the chemically etched Cu_2O microcrystals exhibit excellent SERS performance with absorption of 4-ATP at fairly low concentrations. As shown in Fig. 5, these strong SERS signals originated from those Cu_2O microcrystals after ammonium etching. Distinctive SERS signals from individual microcrystals can be easily observed in the Raman map. The distinct Raman signals, acquired from those individual microcrystals, appear at positions of 1004, 1079, 1141, 1189, 1389, 1435, and 1576 cm^{-1}, which are consistent with Raman spectra of adsorbed 4-ATP molecules.[64–66] The peaks at 1141, 1389, and 1435 cm^{-1} were originally assigned to the b_2 modes due to the photo-induced charge transfer mechanism.[56,64,66] However, it has also been reported that those peaks originated from the a_g modes of the dimerized products that were formed due to surface chemical transformation.[64,67] Even though controversial mechanisms still exist for those peak assignments, the SERS sensitivity of etched Cu_2O microcrystals was clearly demonstrated. It should be noted that the enhancement of the SERS signals could be a combination of more adsorption on a larger surface of modified microcrystals, a strong physical enhancement, and chemical interactions between the probe molecules and modified microcrystals. The first factor related to a larger surface area is not an intrinsic property. Although such a mechanism cannot be excluded, we believe that physical enhancement and chemical interaction would play more significant roles in the enhancement of the SERS signals, as discussed in our previous work.[56] Numerical simulations clearly indicated that the intensity of a localized electromagnetic field can be much higher in the vicinity of the Cu_2O materials. Furthermore, the chemical interactions between the probe molecules and the Cu_2O surface were evidenced by the additional Raman peaks which were absent in the normal Raman spectrum of bulk probe molecules. Actually, the strong SERS signals obtained on the etched Cu_2O microcrystals again confirmed those enhancement mechanisms.

A longer etching time makes Cu_2O microcrystals more sensitive in SERS experiments. For samples with 10 min etching, although the scattering in the optical micrograph is weak and the microcrystals look much smaller, the SERS intensities obtained from those microcrystals are even higher than those etched for 5 min. The insets of Fig. 5d–f show three typical SERS spectra obtained from Cu_2O microcrystals under the above-mentioned conditions, where locations were indicated by corresponding colored arrows in a, b, and c, respectively. We selected two distinct Raman peaks for the EF calculation: 1074 cm^{-1} and 1435 cm^{-1}. To simplify the calculation, we assume that the volumes of probe molecules under the laser spots were equal. The EF of Cu_2O microcrystals reacted with ammonium solution (pH = 11.9) for 10 min is 6.66×10^5 (Raman peak at 1074 cm^{-1}) and 5.88×10^6 (Raman peak at 1435 cm^{-1}). Similarly, the high EF for the Raman peak at 1435 cm^{-1} can be attributed to either photo-induced charge transfer or probe molecule dimerization.

The SERS performance of those etched Cu_2O microcrystals was further systematically studied, in regard to the etching time, pH dependence, and SERS uniformity. Several low-density Cu_2O microcrystal films were prepared to significantly eliminate possible aggregation of the microcrystals. Fig. 6a shows typical Raman spectra from individual Cu_2O microcrystals (0.8 mmol L^{-1} 4-ATP) with various etching times. For the original as-synthesized Cu_2O microcrystals, there were only very tiny SERS signals. Distinct SERS signals were observed from Cu_2O microcrystals with 5 min etching. Increasing the etching time resulted in higher SERS peaks. The summary plot in Fig. 6b shows the relationship between SERS intensity and the etching time of Cu_2O microcrystals in ammonium solutions. Under each etching condition, 20 Cu_2O microcrystals were randomly selected and the peak intensities at 1435 cm^{-1} (see Fig. 6a) were used for comparison. It is very obvious that the Raman intensities were increasing with a longer etching time, and the individual Cu_2O microcrystals after 20 min etching displayed the highest SERS performance. The confocal SERS experiments of microcrystals etched beyond 20 min are not practical due to the inability to identify those individual microcrystals in the optical microscopy. The SERS performance of individual Cu_2O microcrystals is slightly varied even under the same etching conditions, which can be related to the heterogeneity of individual microcrystals and their local environment, such as facet orientation and anisotropic etching. The increasing tendency of SERS abilities along the etching time might be dominated by a higher density of Raman hot spots generated from the rough surface and the increased active charge transfer areas on the etched microcrystals.

The etching process and its impact on SERS were further studied *via* conducting the reaction with ammonium solutions with different pH values. The low-density Cu_2O microcrystal films were reacted for 10 min with ammonium solution with pH

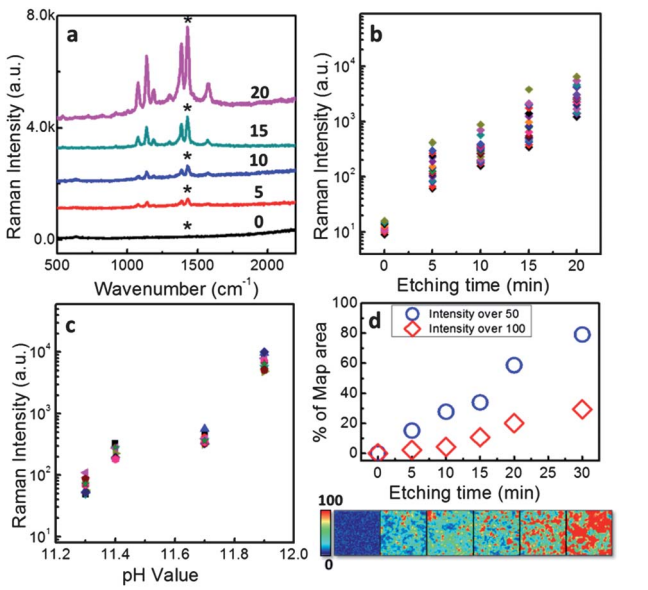

Fig. 6 (a) SERS spectra of 4-ATP molecules adsorbed on individual Cu_2O microcrystals with different reaction times (minutes); (b) statistics of SERS intensities attained from 20 microcrystals under different reaction conditions; (c) statistics of SERS intensities of 10 microcrystals, etched under different pH values for 10 minutes. (d) Statistics of the percentage of intensities in the map area. Raman maps (50 × 50 μm) of high-density Cu_2O microcrystal films that were etched by $NH_3 \cdot H_2O$ solution under different reaction times.

values varying from 11.3 to 11.9. Raman spectra from random individual Cu_2O microcrystals were taken and the dependence of SERS intensity (Raman peak at 1435 cm^{-1}) on the pH of etching solution was studied. The SERS performance of those individual Cu_2O microcrystals is plotted in Fig. 6c. It reveals that the SERS activities of the etched Cu_2O microcrystals were highly sensitive to a small change in the pH value of the etchant. This is usual considering the strong structure–property relationship of the Cu_2O SERS active materials. Altering the etching condition allows tuning of nano- and micro-structures of the products, thus optimizing the SERS performance of final substrates.

The SERS behavior of etched Cu_2O microcrystals was also explored on high-density Cu_2O microcrystal thin films. These films were fabricated *via* a Langmuir–Blodgett method and then they were treated with $NH_3 \cdot H_2O$ solution (pH = 11.7) for different periods of time. Dark field photographs (Fig. S2†) show the comparison of color difference between the original thin film and the one after 20 min etching. Besides the color change, the microcrystal density of the thin film decreased, which is consistent with the UV-Vis results discussed above. Raman maps with a size of 50 × 50 μm were obtained. We found that the Cu_2O microcrystal thin films, similar to the individual Cu_2O microcrystals, revealed a comparable trend of increasing SERS signals when treated for a longer time with $NH_3 \cdot H_2O$ solution. Furthermore, the percentage of the map area (intensities above 50 and 100 counts, respectively) is shown in Fig. 6d. With a longer etching process, Cu_2O microcrystal thin films showed an increase in SERS sensitivity. The long-term SERS sensitivity of the etched Cu_2O microcrystal thin films was also investigated. A Cu_2O microcrystal thin film (with 20 min etching) was measured for Raman intensity for 10 days. As shown in Fig. S3,† the film represented similar Raman enhancements in an acceptable range during those 10 days.

One additional intriguing phenomenon we observed during the chemical etching is that the etching progress and SERS activity also depend on the local microenvironment, such as the packing density of the Cu_2O microcrystals. To investigate such an effect, we fabricated Cu_2O microcrystal thin films *via* a drop-casting method, in which some packed areas were observed with some satellite-like isolated crystals surrounding them. This film was chemically etched *via* ammonium solution (pH = 11.7) for 5 min, and then thoroughly washed before the probe loading. Fig. 7a shows a dark field optical photograph of Cu_2O microcrystals where an area of high-density microcrystals reveals a reddish color whereas some smaller bluish particles localized around the packed area. The different appearance in the dark field image indicates dissimilar etching conditions. The isolated microcrystals were more strongly etched than those of the packed ones, which can lead to a rougher surface, smaller sizes, and weaker reflectance. On the black-white channel image, processed with ImageJ software, the size differences between those packed and isolated crystals are distinguished more easily (Fig. 7b).

The Raman mapping was conducted in the same area and a typical result is shown in Fig. 7c. The SERS signals were obtained from all the etched Cu_2O microcrystals. It is noteworthy that the SERS intensities at most isolated crystals (green circles in the black-white channel image) are stronger than those acquired from close-packed areas. Such a difference in SERS sensitivity is correlated well with the results of a dark-field image, and can be attributed to the different etching conditions for the isolated and close-packed Cu_2O microcrystals. We have mentioned that a slight pH change can cause different etching conditions. The stronger SERS sensitivity of isolated Cu_2O microcrystals might be related to the easy access of chemical regents in the etching solution, thus causing a faster etching reaction as compared to the close-packed ones. Our results confirmed the importance of controlling experimental conditions in preparing etched Cu_2O microcrystals for desired structures and better SERS sensitivities. As compared with other nanoparticles of copper and its oxides, the etched Cu_2O microparticles possess several obvious advantages: well-shaped single crystals with excellent crystallinity; rich history on synthetic approaches for various microscale morphologies; and tunable etching methods for SERS active products. While some of the chemical enhancement mechanisms could be shared with other copper-based SERS substrates, the etched Cu_2O microcrystals have demonstrated excellent SERS sensitivities, thus they have great potentials for designing novel materials with multiple functionalities.

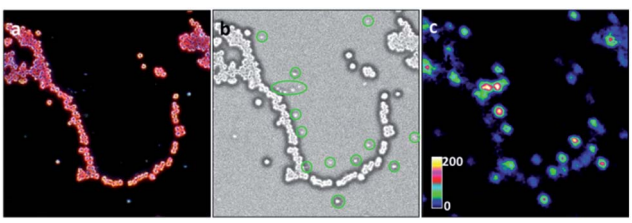

Fig. 7 (a) Dark-field image of the selected featured area from the Cu_2O microcrystal thin film etched in ammonium solution (pH = 11.7) for 5 min, image size: 50 × 50 μm; (b) the same area under the black-white channel, isolated crystals are circled in green; (c) Raman map of the same area.

Conclusion

Cuprous oxide microcrystals etched with an ammonium solution can result in the changes of both structure and chemical composition of the microcrystals. The etching process generated smaller and rougher features on those microcrystals, and strong SERS activity has been observed from the etched microcrystals. The relationship between the SERS sensitivity and etching process was systematically explored. Using this chemical etching approach, the SERS signals from the Cu_2O microcrystals were significantly improved with an enhancement factor up to 10^6. The improvement of SERS ability might be dominated by a higher density of Raman hot spots and the increased area of active charge transfer on etched microcrystals. Both the etching process and the SERS activities varied significantly with the etching time, the pH of the etching solution, and the local chemical microenvironment of the Cu_2O microcrystals. Our work demonstrated a new approach to create SERS-active semiconductor materials and broaden the applications of Cu_2O microcrystals.

Acknowledgements

This work was supported by the National Science Foundation (award number: EPS-0903804 and DGE-0903685), NASA (Cooperative Agreement number: NNX10AN34A), and by the State of South Dakota. Some TEM work was conducted on the instrument funded by the NSF CHE-0840507 grant. Part of the characterization was supported by the Characterization Facility, University of Minnesota, which receives partial support from NSF through the MRSEC Program DMR-0819885. Purchase of the LB trough was made possible through the US Department of Energy, contract number DE-EE0000270. We thank Drs Jason Myers, Bing Luo, and John Nelson for sample characterizations and valuable discussions.

Notes and references

1 H. M. Wei, H. B. Gong, L. Chen, M. Zi and B. Q. Cao, *J. Phys. Chem. C*, 2012, **116**, 10510.
2 D. Cao, C. Wang, F. Zheng, W. Dong, L. Fang and M. Shen, *Nano Lett.*, 2012, **12**, 2803.
3 C. M. McShane, W. P. Siripala and K.-S. Choi, *J. Phys. Chem. Lett.*, 2010, **1**, 2666.
4 Y. Wang, Y.-n. Zhang, G. Zhao, H. Tian, H. Shi and T. Zhou, *ACS Appl. Mater. Interfaces*, 2012, **4**, 3965.
5 M. Leng, M. Liu, Y. Zhang, Z. Wang, C. Yu, X. Yang, H. Zhang and C. Wang, *J. Am. Chem. Soc.*, 2010, **132**, 17084.
6 S. Deng, V. Tjoa, H. M. Fan, H. R. Tan, D. C. Sayle, M. Olivo, S. Mhaisalkar, J. Wei and C. H. Sow, *J. Am. Chem. Soc.*, 2012, **134**, 4905.
7 J.-H. Zhong, G.-R. Li, Z.-L. Wang, Y.-N. Ou and Y.-X. Tong, *Inorg. Chem.*, 2010, **50**, 757.
8 S. Sun, F. Zhou, L. Wang, X. Song and Z. Yang, *Cryst. Growth Des.*, 2009, **10**, 541.
9 Y. Zhang, B. Deng, T. Zhang, D. Gao and A.-W. Xu, *J. Phys. Chem. C*, 2010, **114**, 5073.
10 Y. Xu, H. Wang, Y. Yu, L. Tian, W. Zhao and B. Zhang, *J. Phys. Chem. C*, 2011, **115**, 15288.
11 W.-C. Huang, L.-M. Lyu, Y.-C. Yang and M. H. Huang, *J. Am. Chem. Soc.*, 2011, **134**, 1261.
12 Y. Tan, X. Xue, Q. Peng, H. Zhao, T. Wang and Y. Li, *Nano Lett.*, 2007, **7**, 3723.
13 Z. Zhang, H. Che, Y. Wang, J. Gao, L. Zhao, X. She, J. Sun, P. Gunawan, Z. Zhong and F. Su, *Ind. Eng. Chem. Res.*, 2011, **51**, 1264.
14 H. Xu, W. Wang and L. Zhou, *Cryst. Growth Des.*, 2008, **8**, 3486.
15 L. Zhang and H. Wang, *ACS Nano*, 2011, **5**, 3257.
16 Z. Zheng, B. Huang, Z. Wang, M. Guo, X. Qin, X. Zhang, P. Wang and Y. Dai, *J. Phys. Chem. C*, 2009, **113**, 14448.
17 J. Fang, S. Lebedkin, S. Yang and H. Hahn, *Chem. Commun.*, 2011, **47**, 5157.
18 V. Yathindranath, L. Rebbouh, D. F. Moore, D. W. Miller, J. van Lierop and T. Hegmann, *Adv. Funct. Mater.*, 2011, **21**, 1457.
19 J. C. Park, J. Kim, H. Kwon and H. Song, *Adv. Mater.*, 2009, **21**, 803.
20 Z. Wang, D. Luan, F. Y. C. Boey and X. W. Lou, *J. Am. Chem. Soc.*, 2011, **133**, 4738.
21 C. C. Yec and H. C. Zeng, *Chem. Mater.*, 2012, **24**, 1917.
22 M. Ofuji, A. J. Lovinger, C. Kloc, T. Siegrist, A. J. Maliakal and H. E. Katz, *Chem. Mater.*, 2005, **17**, 5748.
23 P. V. Kamat, *J. Phys. Chem. Lett.*, 2011, **2**, 2832.
24 G. Ashkenasy, D. Cahen, R. Cohen, A. Shanzer and A. Vilan, *Acc. Chem. Res.*, 2002, **35**, 121.
25 M. D. Regulacio and M.-Y. Han, *Acc. Chem. Res.*, 2010, **43**, 621.
26 L. Jiang, T. You, P. Yin, Y. Shang, D. Zhang, L. Guo and S. Yang, *Nanoscale*, 2013, **5**, 2784.
27 L. Zhang, X. Gong, Y. Bao, Y. Zhao, M. Xi, C. Jiang and H. Fong, *Langmuir*, 2012, **28**, 14433.
28 J. R. Lombardi and R. L. Birke, *Acc. Chem. Res.*, 2009, **42**, 734.
29 L. Brus, *Acc. Chem. Res.*, 2008, **41**, 1742.
30 A. E. Aliaga, T. Aguayo, C. Garrido, E. Clavijo, E. Hevia, J. S. Gómez-Jeria, P. Leyton, M. M. Campos-Vallette and S. Sanchez-Cortes, *Biopolymers*, 2011, **95**, 135.
31 S. M. Ansar, X. Li, S. Zou and D. Zhang, *J. Phys. Chem. Lett.*, 2012, **3**, 560.
32 R. A. Halvorson and P. J. Vikesland, *Environ. Sci. Technol.*, 2010, **44**, 7749.
33 R. Kodiyath, S. T. Malak, Z. A. Combs, T. Koenig, M. A. Mahmoud, M. A. El-Sayed and V. V. Tsukruk, *J. Mater. Chem. A*, 2013, **1**, 2777.
34 Y. Bao, C. Lai, Z. Zhu, H. Fong and C. Jiang, *RSC Adv.*, 2013, **3**, 8998–9004.
35 N. L. Netzer, C. Qiu, Y. Zhang, C. Lin, L. Zhang, H. Fong and C. Jiang, *Chem. Commun.*, 2011, **47**, 9606.
36 Y. Liu, Y. Zhang, H. Ding, S. Xu, M. Li, F. Kong, Y. Luo and G. Li, *J. Mater. Chem. A*, 2013, **1**, 3362.
37 L. Lu and A. Eychmüller, *Acc. Chem. Res.*, 2008, **41**, 244.
38 A. Samanta, K. K. Maiti, K.-S. Soh, X. Liao, M. Vendrell, U. S. Dinish, S.-W. Yun, R. Bhuvaneswari, H. Kim, S. Rautela, J. Chung, M. Olivo and Y.-T. Chang, *Angew. Chem., Int. Ed.*, 2011, **50**, 6089.
39 W. R. Premasiri, D. T. Moir, M. S. Klempner, N. Krieger, G. Jones and L. D. Ziegler, *J. Phys. Chem. B*, 2004, **109**, 312.
40 C. Garrido, A. E. Aliaga, J. S. Gomez-Jeria, R. E. Clavijo, M. M. Campos-Vallette and S. Sanchez-Cortes, *J. Raman Spectrosc.*, 2010, **41**, 1149.
41 S. A. Meyer, E. C. L. Ru and P. G. Etchegoin, *J. Phys. Chem. A*, 2010, **114**, 5515.
42 S. Thomas, N. Biswas, S. Venkateswaran, S. Kapoor, S. Naumov and T. Mukherjee, *J. Phys. Chem. A*, 2005, **109**, 9928.
43 M. Rycenga, P. H. C. Camargo, W. Li, C. H. Moran and Y. Xia, *J. Phys. Chem. Lett.*, 2010, **1**, 696.
44 C. Farcau and S. Astilean, *J. Phys. Chem. C*, 2010, **114**, 11717.
45 Z.-Q. Tian and B. Ren, in *Encyclopedia of Electrochemistry*, Wiley-VCH Verlag GmbH & Co. KGaA, 2007.
46 Z.-Q. Tian, B. Ren and D.-Y. Wu, *J. Phys. Chem. B*, 2002, **106**, 9463.
47 A. Musumeci, D. Gosztola, T. Schiller, N. M. Dimitrijevic, V. Mujica, D. Martin and T. Rajh, *J. Am. Chem. Soc.*, 2009, **131**, 6040.

48 X. Wang, W. Shi, G. She and L. Mu, *J. Am. Chem. Soc.*, 2011, **133**, 16518.
49 J. M. Luther, P. K. Jain, T. Ewers and A. P. Alivisatos, *Nat. Mater.*, 2011, **10**, 361.
50 S.-W. Hsu, K. On and A. R. Tao, *J. Am. Chem. Soc.*, 2011, **133**, 19072.
51 A. Kudelski, W. Grochala, M. Janik-Czachor, J. Bukowska, A. Szummer and M. Dolata, *J. Raman Spectrosc.*, 1998, **29**, 431.
52 R.-C. Wang and H.-Y. Lin, *Mater. Chem. Phys.*, 2012, **136**, 661.
53 R.-C. Wang and C.-H. Li, *Acta Mater.*, 2011, **59**, 822.
54 Y. Wang, W. Song, W. Ruan, J. Yang, B. Zhao and J. R. Lombardi, *J. Phys. Chem. C*, 2009, **113**, 8065.
55 Y. Wang and T. Asefa, *Langmuir*, 2010, **26**, 7469.
56 C. Qiu, L. Zhang, H. Wang and C. Jiang, *J. Phys. Chem. Lett.*, 2012, **3**, 651.
57 Z. Yang, S. Sun, C. Kong, X. Song and B. Ding, *J. Nanomater.*, 2010, **2010**, 710584.
58 S. L. Westcott, J. B. Jackson, C. Radloff and N. J. Halas, *Phys. Rev. B: Condens. Matter Mater. Phys.*, 2002, **66**, 155431.
59 L. Zhang and H. Wang, *J. Phys. Chem. C*, 2011, **115**, 18479.
60 Q. Hua, K. Chen, S. Chang, Y. Ma and W. Huang, *J. Phys. Chem. C*, 2011, **115**, 20618.
61 C.-K. Wu, M. Yin, S. O'Brien and J. T. Koberstein, *Chem. Mater.*, 2006, **18**, 6054.
62 C. C. Chusuei, M. A. Brookshier and D. W. Goodman, *Langmuir*, 1999, **15**, 2806.
63 M. Yin, C.-K. Wu, Y. Lou, C. Burda, J. T. Koberstein, Y. Zhu and S. O'Brien, *J. Am. Chem. Soc.*, 2005, **127**, 9506.
64 D.-Y. Wu, X.-M. Liu, Y.-F. Huang, B. Ren, X. Xu and Z.-Q. Tian, *J. Phys. Chem. C*, 2009, **113**, 18212.
65 M. Sun, Y. Huang, L. Xia, X. Chen and H. Xu, *J. Phys. Chem. C*, 2011, **115**, 9629.
66 Z. Mao, W. Song, L. Chen, W. Ji, X. Xue, W. Ruan, Z. Li, H. Mao, S. Ma, J. R. Lombardi and B. Zhao, *J. Phys. Chem. C*, 2011, **115**, 18378.
67 B. Dong, Y. Fang, X. Chen, H. Xu and M. Sun, *Langmuir*, 2011, **27**, 10677.